Hydrogenation-induced Structural Change and Spin-Reorientation Transition

Wen-Chin Lin
Department of Physics, National Taiwan Normal University, Taipei 11677, Taiwan.
Email: wclin@ntnu.edu.tw

Hydride formation on magnetic properties of Pd/Co/Mg

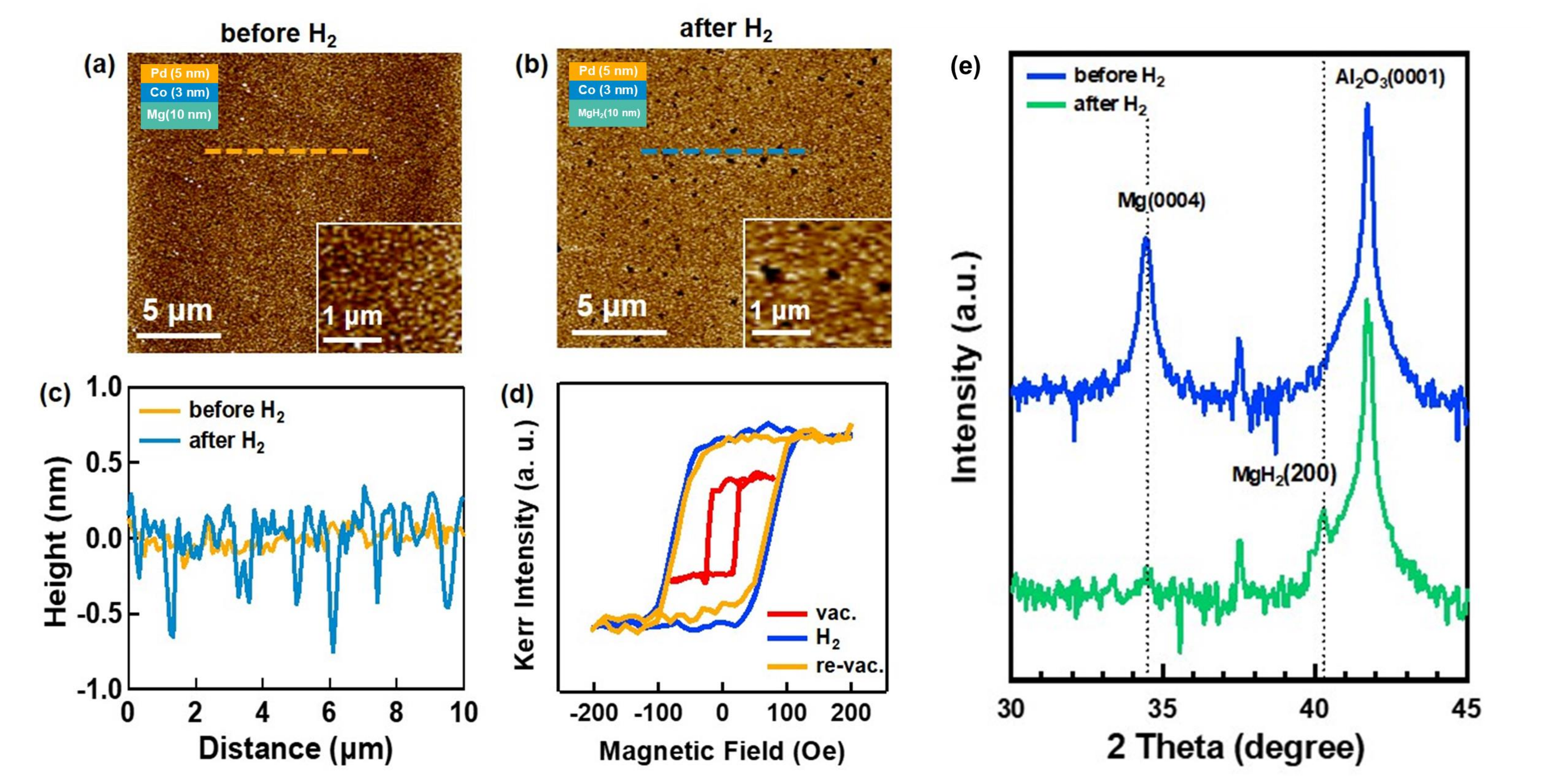

AFM image of the Pd(5 nm)/Co(3 nm)/Mg(10 nm) multilayer (a) before and (b) after 1 bar H_2 gas exposure. (c) The line profiles, as indicated in (a) and (b), revealing a significantly enhanced surface corrugation and roughness after H exposure. (d) The MOKE hysteresis loops for the multilayer in vacuum, during H_2 exposure, and after returning to the vacuum. (e) Crystalline structure of sample characterized by XRD before and after exposure to 1 bar H_2 gas.

Surfaces and Interfaces 36 (2023) 102503

Hydrogenation on magnetotransport properties of Pd/Co/Mg/Fe

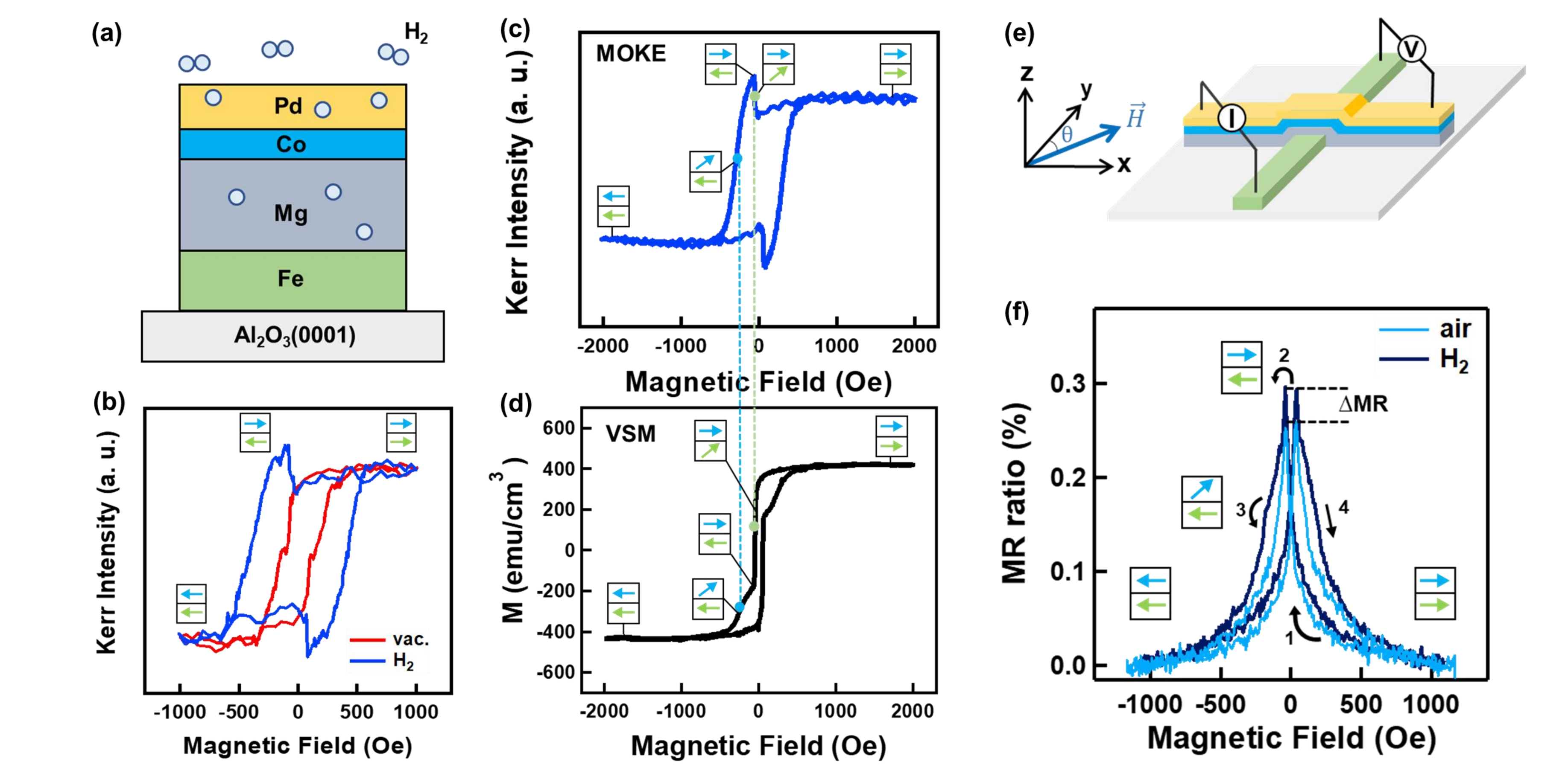

(a) and (b) MOKE hysteresis loops in vacuum and a H_2 environment in Pd(5 nm)/Co(3 nm)/Mg(25 nm)/Fe(10 nm). (c) and (d) MOKE and VSM hysteresis loops of the sample in air after absorbing 1 bar H_2 gas at RT. (e) Schematic of the MR measurement configuration. (f) MR curve before and after hydrogenation of the multilayer sample.

ACS Omega 2023, 8, 30, 26948–26954

Hydrogen-Controlled Anisotropy in FePd/Co/[Pt/Co]$_4$/Pt

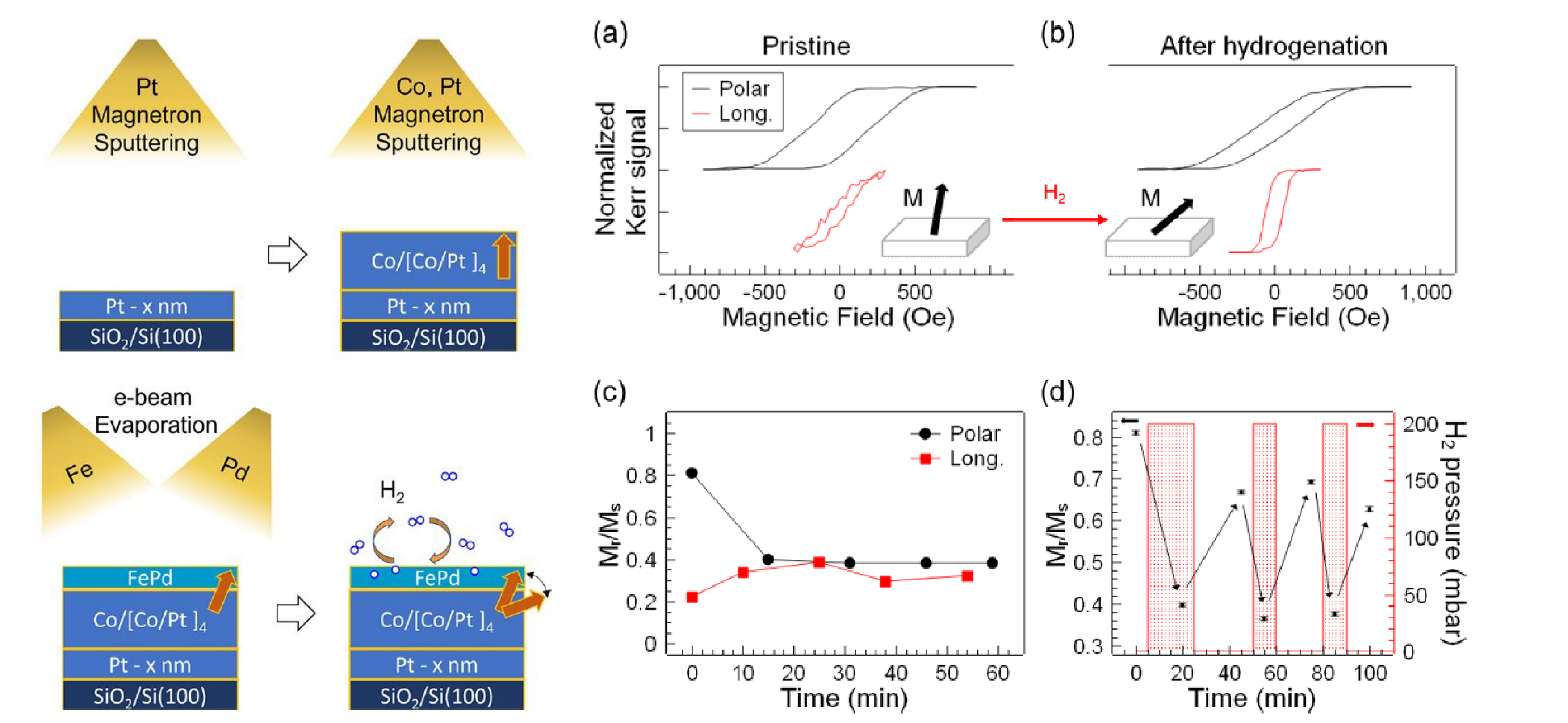

Schematic illustrations for the sample structure, fabrication processes, and hydrogen absorption-induced changes in magnetism. Polar and longitudinal MOKE hysteresis loops of 2 nm FePd/Co (0.3 nm)/[Pt (0.8 nm)/Co (0.3 nm)]$_4$/Pt(2 nm) (a) before, and (b) after hydrogenation. (c) The M_r/M_s ratios of polar and longitudinal Kerr signals are plotted as a function of time in H_2 gas of 200 mbar. (d) The M_r/M_s ratio plotted as a function of time with cyclic changes in gas pressure between a vacuum of 5×10^{-3} mbar and H_2 gas of 200 mbar, which is exhibited by the shadow color corresponding to the right axis.

ACS Appl. Nano Mater. 2023, 6, 2784−2790

Hydrogen-Controlled Anisotropy in Pd/[Co/Pd]$_8$/Pd

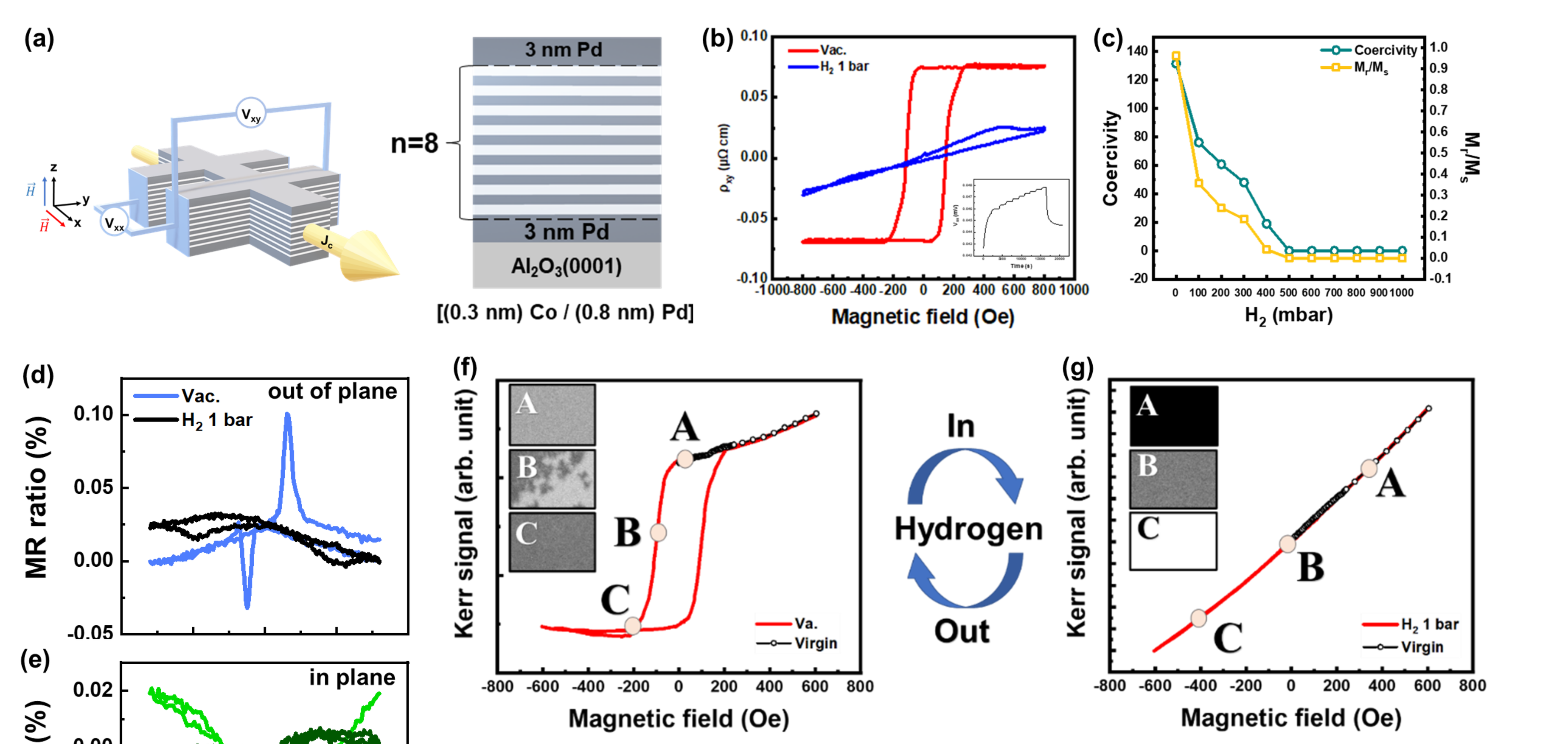

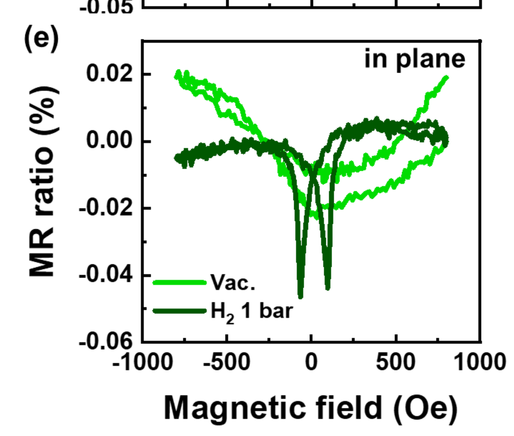

(a) Illustrations for the sample structure and measurement geometry. (b), (c) The hysteresis curves were measured by AHE under various hydrogen pressures. (d), (e) The out-of-plane and in-plane MR curves before and after the hydrogenation effect. (f), (g) The reversible magnetic change by hydrogenation effect through Kerr microscope.

Manuscript in preparation

Field-free magnetic rotation in FePd alloy films controlled by reversible hydrogenation

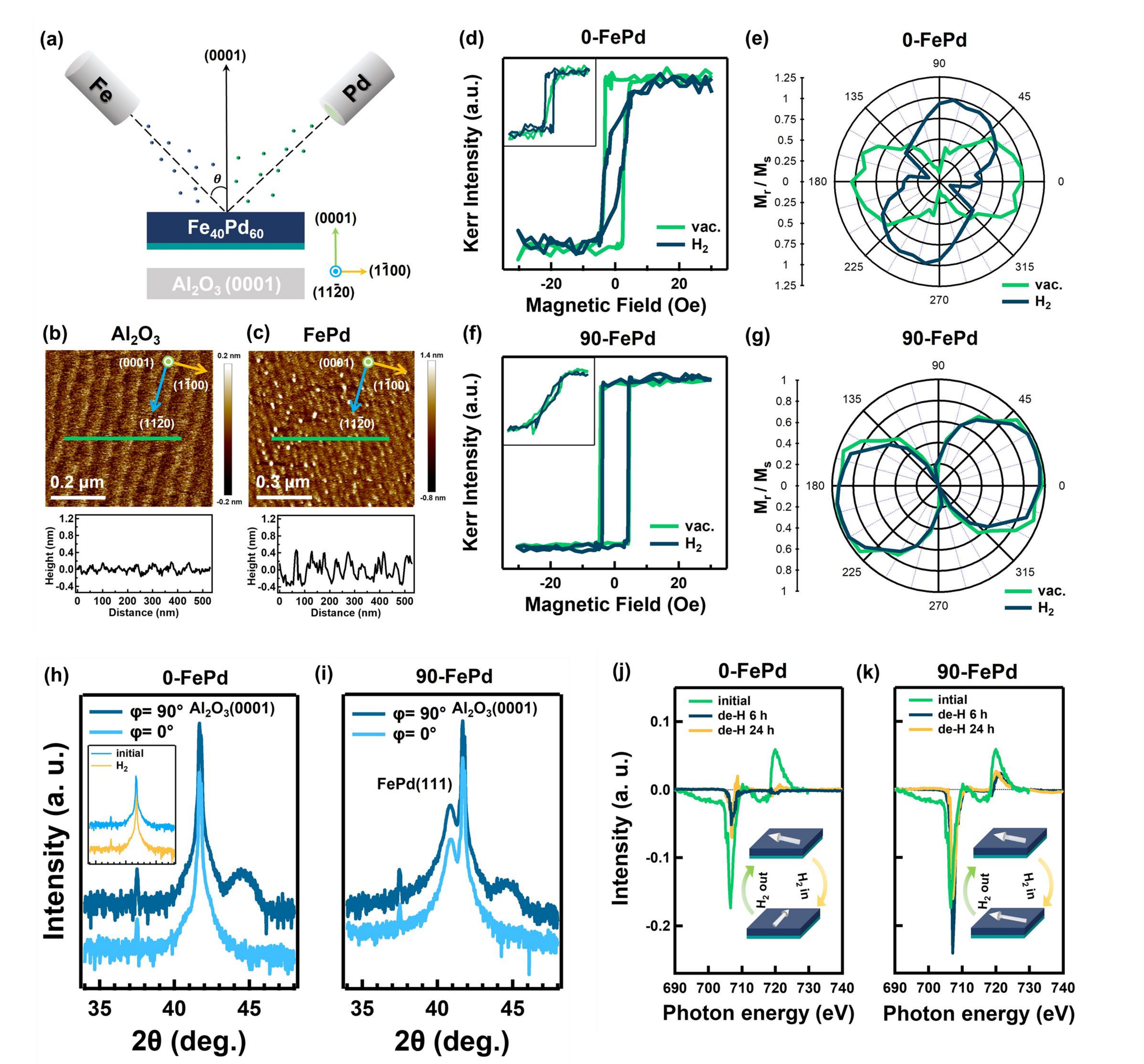

(a) Growth geometry of 0-FePd alloy. (b), (c) The AFM observation reveals the surface morphology of the substrate and FePd 1D micro-ripples. (d), (f) Hysteresis loops were measured before and after hydrogenation effect. (e), (g) Polar plots of M_r/M_s before and after hydrogen absorption. (h), (i) The XRD spectra of FePd alloy. (j), (k) The XMCD spectra of FePd thin film under a vacuum of 1×10^{-9} mbar for initial state, 6 h, and 24 h after exposure to 1 bar hydrogen gas.

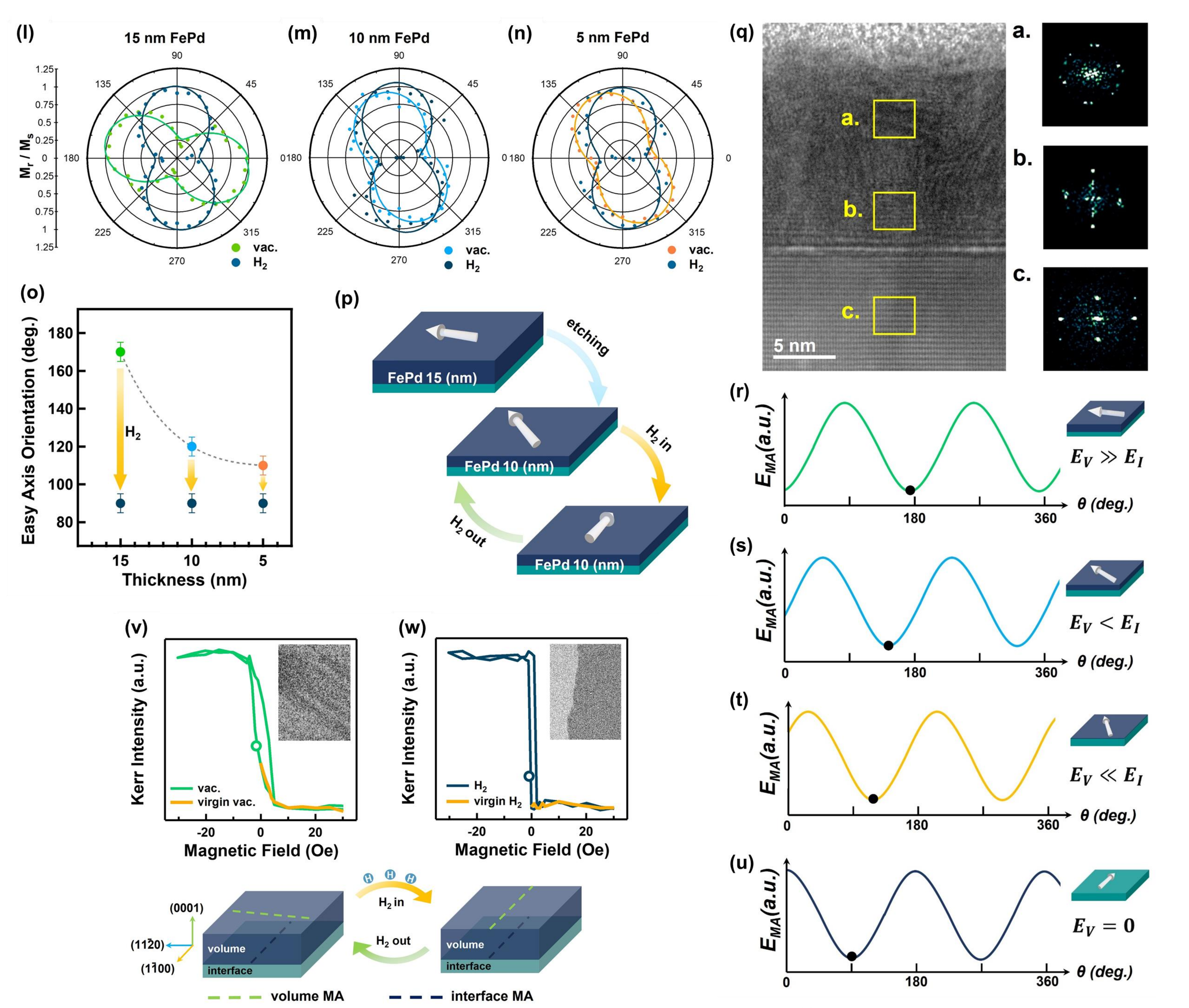

(l)-(n) The change in MA of FePd alloy film with the hydrogenation effect and etching treatments. (o), (p) Regardless of the etching duration, the MA direction consistently undergoes a transition to 90° upon hydrogenation and corresponds to the light grey magnetic moment reorientation. (q) The crystal lattice arrangement in different regions is revealed in the TEM. (r)-(u) When the film thickness is higher, it is dominated by E_V, and when the film thickness is thinner, it is dominated by E_I. (v), (w) Field-free switching in FePd thin film through the absorption and desorption of hydrogen.

Manuscript in preparation